

pubs.acs.org/acssensors Article

Laser-Induced Graphene Electrochemical Immunosensors for Rapid and Label-Free Monitoring of Salmonella enterica in Chicken Broth

Raquel R. A. Soares, Robert G. Hjort, Cicero C. Pola, Kshama Parate, Efraim L. Reis, Nilda F. F. Soares, Eric S. McLamore, Jonathan C. Claussen,* and Carmen L. Gomes*



Cite This: https://dx.doi.org/10.1021/acssensors.9b02345



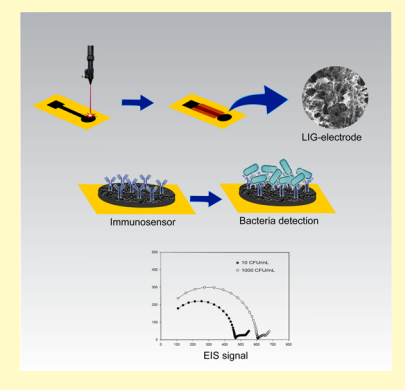
ACCESS

Metrics & More

Article Recommendations

Supporting Information

ABSTRACT: Food-borne illnesses are a growing concern for the food industry and consumers, with millions of cases reported every year. Consequently, there is a critical need to develop rapid, sensitive, and inexpensive techniques for pathogen detection in order to mitigate this problem. However, current pathogen detection strategies mainly include time-consuming laboratory methods and highly trained personnel. Electrochemical in-field biosensors offer a rapid, low-cost alternative to laboratory techniques, but the electrodes used in these biosensors require expensive nanomaterials to increase their sensitivity, such as noble metals (e.g., platinum, gold) or carbon nanomaterials (e.g., carbon nanotubes, or graphene). Herein, we report the fabrication of a highly sensitive and label-free laser-induced graphene (LIG) electrode that is subsequently functionalized with antibodies to electrochemically quantify the food-borne pathogen *Salmonella enterica* serovar Typhimurium. The LIG electrodes were produced by laser induction on the polyimide film in ambient conditions and, hence, circumvent the need for high-temperature, vacuum environment, and metal seed



catalysts commonly associated with graphene-based electrodes fabricated via chemical vapor deposition processes. After functionalization with Salmonella antibodies, the LIG biosensors were able to detect live Salmonella in chicken broth across a wide linear range (25 to 10^5 CFU mL⁻¹) and with a low detection limit (13 ± 7 CFU mL⁻¹; n = 3, mean \pm standard deviation). These results were acquired with an average response time of 22 min without the need for sample preconcentration or redox labeling techniques. Moreover, these LIG immunosensors displayed high selectivity as demonstrated by nonsignificant response to other bacteria strains. These results demonstrate how LIG-based electrodes can be used for electrochemical immunosensing in general and, more specifically, could be used as a viable option for rapid and low-cost pathogen detection in food processing facilities before contaminated foods reach the consumer.

KEYWORDS: graphene, biosensor, electrochemical impedance spectroscopy, foodborne pathogens, food safety, Salmonella Typhimurium

Tearly half a million people die each year from acquiring food-borne illnesses. This dismal statistic is only expected to increase as global food production, and the trade continues to rise to meet the demands of the increasing world population (over 9 billion by 2050 according to the United Nations prediction²). Hence, efficient food quality control measures are desperately needed to avoid wide-spread foodborne diseases and contamination. Data from Food and Drug Administration (FDA) and Centers for Disease Control and Prevention (CDC) claim that one of the major contributors to food-borne illnesses is the bacteria Salmonella enterica, which causes about 1.2 million illnesses, 23,000 hospitalizations, and 450 deaths in the United States every year.^{3,4} Furthermore, Salmonella causes an estimated \$3.7 billion in economic burdens each year with exposure occurring through food, water, and contaminated surfaces.⁵ Despite strict regulations and efforts from producers to control pathogens in the food supply, growing numbers of food-borne illnesses are being reported globally.6

The reason for these illnesses is that the contaminated food product (whether contaminated in the field or within food processing facilities) still passes unnoticed to the consumer. This is because food-borne pathogen detection is time-consuming and arduous. The gold standards for monitoring these pathogens include bacteria plate counting and polymerase chain reaction (PCR) experiments that may take several days because of pre-enrichment steps and necessary laboratory processing. Hence, all food products passing through the doors of food processing facilities are not tested for pathogens as some food would spoil before tests could be performed, and most food products have low/tight profit margins making ubiquitous testing infeasible. Therefore, there is an urgent

Received: November 26, 2019 Accepted: April 15, 2020



need to create rapid (less than 1 h), low-cost (less than \$1), and highly sensitive (detection limits comparable to plate counting and PCR methods) sensor systems that can be used on-site to detect food-borne pathogens such as *Salmonella*. ^{10,11} Recent research into electrochemical biosensors, including our own, ^{12–16} has demonstrated promising potential for such infield pathogen and containment detection. ^{17–19}

Electrochemical biosensors have been explored extensively in recent years as an alternative to conventional methods for detection of pathogenic bacteria, mainly because of their high sensitivity, easy handling, fast response time, and low costs. 20-23 Moreover, comparing them with other commonly used techniques, such as colorimetric and fluorescence assays, electrochemical transducers have significant advantages because they do not require laborious interpretation and equipment resources, exhibit more versatile detection schemes which provide broader applications, and are capable of realtime quantification. 24,25 Also, electrochemical biosensors have received particular attention because they can perform direct and label-free measurements and can be easily manipulated by the personnel without previous training (e.g., home glucose monitors for diabetics^{26,27}). Moreover, electrochemical biosensors that are modified with carbon nanomaterials such as graphene have significantly improved biosensor performance^{28,29} and have increasingly been applied to food safety and sustainable agriculture applications. Recent reports have demonstrated potential in developing sensitive and accurate electrochemical Salmonella detection platforms. 24,31-33 However, some of these biosensors are complex and costly because they require expensive (noble metals 34,35) or difficult to fabricate materials (e.g., gold nanoparticles biofunctionalized with enzymes;³⁶ nanocomposites using graphene oxide and titanium isopropoxide³⁷) to improve signal amplification and/or complex manufacturing steps (e.g., cleanroom processing³⁸). It should also be noted that the main challenge in the field of biosensing for monitoring pathogens is not the response time but the poor detection limit, approximately 10^2 to 10^3 CFU mL⁻¹ (detection limits of ≤ 5 CFU mL⁻¹ are required for ensuring pathogen-free food products 10,17). To overcome this hurdle, most studies have integrated a preconcentration step, which improves detection limit but obfuscates the rationale for creating the rapid sensor in the first place. However, a graphene biosensor may help to overcome these detection limit shortcomings by improving the sensor sensitivity.

Within the category of two-dimension materials, graphene is considered outstanding because of its structure and exceptional properties. 39,40 Graphene is a sheet of sp²-bonded carbon atoms arranged into a rigid hexagonal lattice, exhibiting a set of properties that no material has concomitantly displayed, for example, high mechanical strength (10¹² Pa), excellent electrical conductivity and charge carrier mobility (~10⁵ cm² V^{-1} s⁻¹), large specific surface area (~2630 m² g⁻¹), and high impermeability and biocompatibility.⁴¹⁻⁴³ Consequently, graphene-like nanomaterials have attracted attention as emerging materials for electrochemical sensor applications.⁴⁴ Techniques for graphene electrode fabrication have grown considerably to supply the demand for this material;³⁹ however, common methods of synthesis, such as photolithography 45,46 (an expensive cleanroom processing technique), chemical vapor deposition (CVD),⁴⁷ and laser ablation,⁴⁸ include high thermal requirements, low-pressure (vacuum) requirements, or multiple steps toward chemical formation of graphene.⁴⁹ Moreover, postsynthesis processing is generally required to transfer the graphene to a nonconductive substrate,⁵⁰ which further increases the time and cost of electrode fabrication. An alternative to these expensive graphene electrode fabrication techniques is to produce sensors based on direct-write processes such as inkjet printing or aerosol jet printing that are capable of printing graphene electrodes from graphene flakes synthesized from bulk chemical exfoliation of graphite. 51-54 Though these graphene electrode fabrication methods do not retain the highperformance characteristics of pristine CVD-grown graphene, for example, they do display sufficient electrical conductivity and biocompatibility needed for a variety of sensor applications and eliminate the high cost of alternative graphene synthesis protocols and graphene transfer methods. However, these printing techniques often require additional postprint processing (e.g., laser, 53 thermal, 55 or photonic annealing 56) to increase the electrical conductivity of the printed graphene, which further complicates their fabrication process.

As an alternative to these techniques, the Tour group 49 introduced a simple one-step, direct-write graphene electrode fabrication method, called laser-induced graphene (LIG). LIG is typically formed by converting sp³ carbon found in polyimide (PI) into highly conductive sp²-hybridized carbon found in graphene through CO₂ laser induction^{57,58} (though some have demonstrated LIG formation on PI using a UV laser^{59,60}). LIG combines both the graphene synthesis and graphene electrode fabrication steps into one simple process, using a laser to selectively convert distinct patterns of PI into a high-surface graphene circuit that is often nano/microstructured or porous. Because LIG can be easily manufactured from commercial polymers, it has been applied toward stretchable and sensitive strain gauges,⁶¹ nonbiofouling surfaces,⁶² microsupercapacitors,⁶³ UV photodetectors,⁶⁴ sound generators and detectors,⁶⁵ and more recently, electrochemical sensors.⁶⁶ Recently, an electrochemical biosensor based on LIG electrodes has been developed for the detection of biogenic amines in food samples; 59 similarly, in another study, an electrochemical biosensor was developed based on LIG that showed the ability to detect low levels of the antibiotic chloramphenicol, which is banned in food production.³⁵ Another example is the electrochemical LIG sensor used for fouling biofilm detection, one of the main challenges in the food industry⁶² while another LIG sensor was capable of monitoring the concentration of nitrogen (both ammonium and nitrate ions in soil solutions) in the hopes of better monitoring and controlling fertilizer inputs in farm fields to maximize crop yield while lowering fertilizer waterway pollution because of excess fertilizer use. 60 However, electrochemical pathogen sensing using LIG has yet to be demonstrated.

Herein, we report on the first LIG sensor that is capable of rapid and quantifiable detection of *S. enterica* concentrations in food samples. Porous graphene was produced from PI by laser induction and then characterized conferring a new potential application in the sensing field. An impedimetric immunosensor was developed based on LIG electrodes functionalized with specific antibodies for detection of *S. enterica*, one of the most prominent food-borne pathogens. The immunosensor was able to detect the pathogen at low concentration, 13 ± 7 CFU mL⁻¹ in complex media, chicken broth, with a response time of 22 min. Electrochemical impedance spectroscopy (EIS) was used as a label-free detection over a broad range of

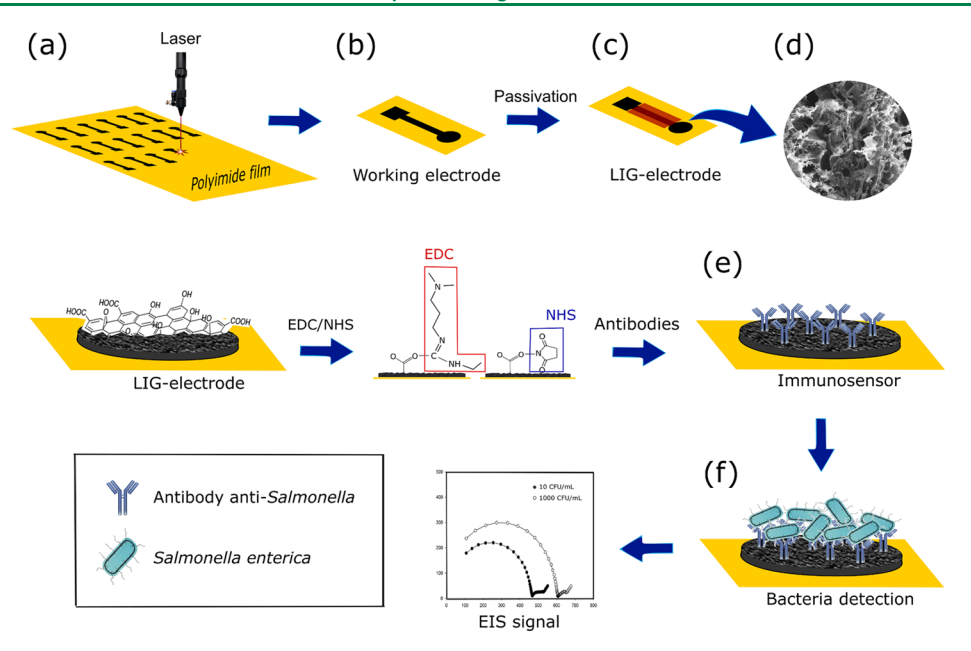


Figure 1. Fabrication, biofunctionalization, and sensing scheme of the LIG immunosensor. Fabrication and biofunctionalization steps included (a) LIG processing onto a polyimide (Kapton) sheet to create the (b) working electrode, (c) passivation of the working electrode with lacquer, (d) SEM image showing the LIG surface, (e) biofunctionalization with *Salmonella* antibodies immobilized on the working electrode via carbodiimide cross-linking chemistry, and (f) *Salmonella* binding to the electrode and the resultant Nyquist plot generated during electrochemical sensing.

bacteria concentrations, from 25 to 10⁵ CFU mL⁻¹. Moreover, this promising device is a low-cost and disposable sensor that can be used in-field or at the point-of-service (e.g., food processing facilities) for the detection of contamination, which reinforces its important contribution to food safety.

MATERIAL AND METHODS

Materials. PI (Kapton, 0.07 mm) tape was purchased from McMaster-Carr co. (Elmherst, IL, USA), and Epson Ultra Premium Photo Luster (240 g m⁻²) was acquired from Office Depot (Boca Raton, FL, USA). Potassium ferro/ferricyanide, N-hydroxysuccinimide (NHS), 1-ethyl-3-(3-dimethylaminopropyl) carbodiimide (EDC), 2-(N-morpholino)ethanesulfonic acid (MES), and ethanolamine were purchased from Sigma-Aldrich (St. Louis, MO, USA). Tryptic soy agar (TSA), tryptic soy broth (TSB), tryptose phosphate broth (TPB), and buffered peptone water (BPW) were purchased from Criterion Dehydrated Culture Media (Hardy Diagnostics, Santa Maria, CA, USA). Potassium chloride and SuperBlock in phosphate buffered saline (PBS) (used as the blocking buffer) were purchased from ThermoFisher Scientific (Waltham, MA, USA). KPL BacTrace polyclonal antibody anti-Salmonella was purchased from SeraCare (USA). PBS was purchased from Alpha Aesar (Tewksbury, MA, USA), and chicken broth was purchased from a local supermarket. All the chemicals used in this study were of analytical grade. Solutions were made using deionized with an electric resistance of approximately 18.2 M Ω .

LIG Electrode Fabrication. The working electrode was designed using a linear sketch pattern (0.17 mm separation) in SolidWorks 2018 (Dassault Systems, France), and the engraving process was performed with a 75 W Epilog Fusion M2 CO₂ laser (Epilog Laser, Golden, CO, USA) at 7% speed and 4% power with a lens to a material distance of ~74 mm and a beam size of ~176 μ m in an ambient atmosphere. The laser induction was carried out on the PI film taped onto the emulsion side of the photo paper, as previously described by Tehrani and Bavarian and Fenzl et al. The working area (3 mm diameter) and connector ends of the working electrode were separated by a layer of fast drying lacquer (passivation layer) used to cover the nonactive areas of the electrodes. Passivation was done to

maintain a constant area of the working electrode in contact with the redox solution during electrochemical sensing. 60

■ MATERIAL CHARACTERIZATION

The Raman spectrum was obtained by using a Renishaw InVia confocal Raman microscope with a 633 nm laser source (0.12 mW), a 50× objective lens, and a diffraction grating of 1800 lines, in order to confirm the graphene formation by the laser induction process. The crystallinity of the bare electrodes and the level of graphitization were evaluated using a Bruker D8 DISCOVER X-ray Diffractometer provided with copper radiation (λ = 1.542 Å) scanning $\theta/2\theta$. A scanning electron microscope (JEOL JSM-6010LA) equipped with an energy dispersive spectroscopy (EDS) system was used to obtain images of the LIG morphology at 230×, 2000×, and 2300× magnification and the electrode chemical composition, at an accelerating voltage of 5 kV.

Antibody Functionalization onto LIG Electrodes. To determine the optimum concentration of polyclonal antibody anti-Salmonella to functionalize the LIG electrodes, different concentrations of antibody were initially functionalized on the electrode surface in an effort to maximize immunosensor performance. Briefly, the working area of the electrodes was covered with 30 μ L of EDC/NHS (3:1) solubilized in sterile filtered MES (pH 6.0) for 1 h and then rinsed with 1× dilution of PBS (1× PBS) pH 7.4 to remove the unreacted EDC/NHS. Next, polyclonal antibody anti-Salmonella at different concentrations (0.5, 1.0, and 1.5 μ M) was applied to the surface of the working electrode, followed by overnight incubation at 4 °C. The electrode was then rinsed with 1× PBS, dried at room temperature, and afterward, 1 M ethanolamine was applied for 20 min to quench the remaining unreacted EDC/NHS. The unreacted graphitic surface was blocked using Superblock in 1× PBS, for 20 min, to reduce nonspecific binding and then rinsed off with 1× PBS, prior to testing.

Electrochemical Characterization. The electrochemical proprieties of the LIG electrodes were analyzed using cyclic

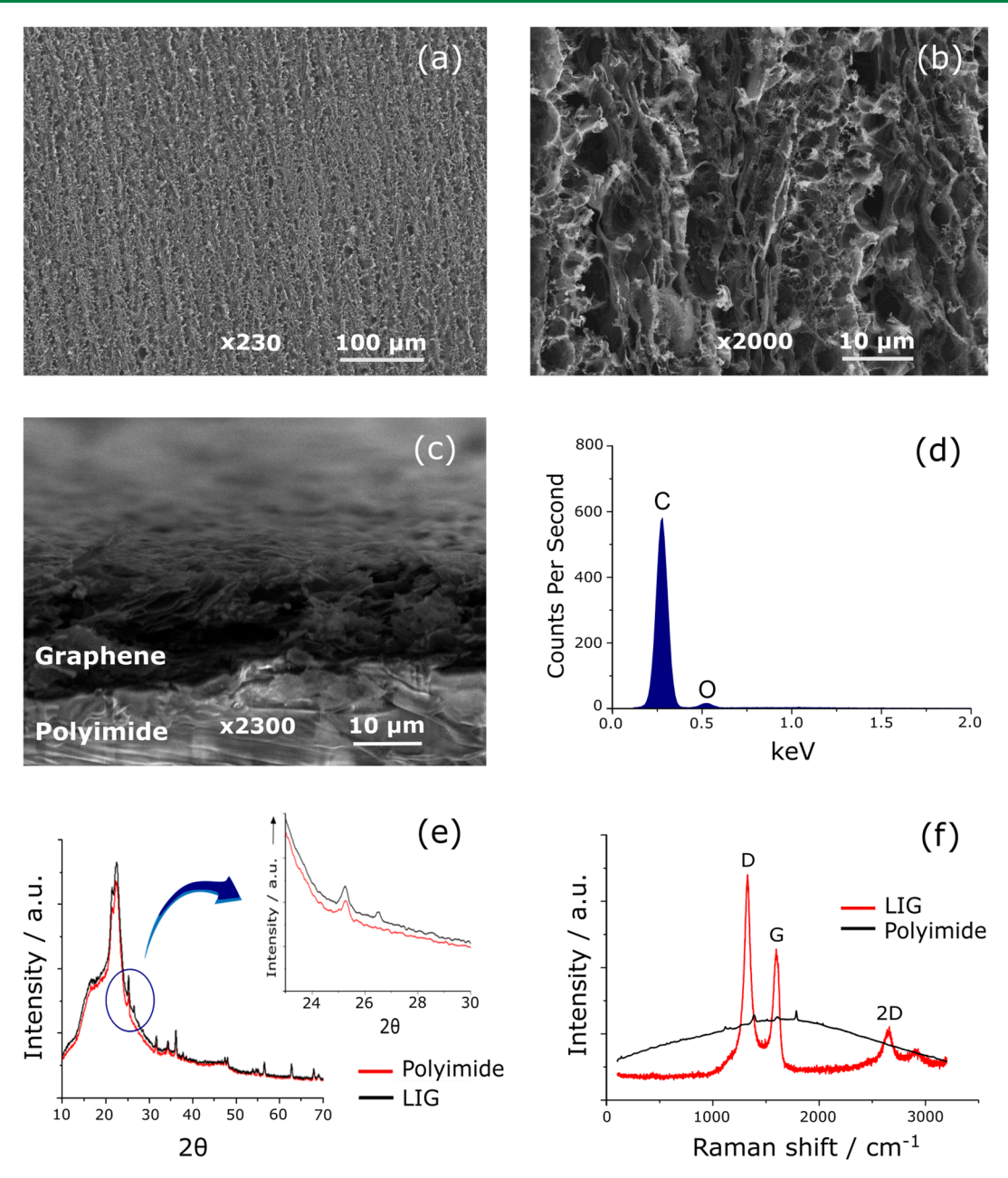


Figure 2. SEM images of the bare LIG electrode at 5 kV, (a) 230×, and (b) 2000× magnification, confirming the porous graphene morphology; (c) SEM cross-sectional image of the same electrode at 5 kV and 2300× magnification; (d) EDS spectrum of the LIG-electrode, showing the predominance of carbon and a small portion of oxygen, indicating the change in chemical composition and chemical bonds after laser processing; (e) representative XRD spectrum comparing PI and LIG, which displays a peak at $2\theta = 26.5^{\circ}$, indicating graphitization; (f) Raman spectrum comparing PI and LIG and showing the three characteristic peaks of graphene D, G, and 2D with a ratio $I_{\rm 2D}/I_{\rm G} \approx 0.35$, which indicates multilayer graphene formation.

voltammetry (CV) and EIS. All electrochemical measurements were carried out on a CH Instruments Electrochemical Analyzer (CHI7081E model, CH Instruments, Inc., Austin, TX, USA) at room temperature. The three-electrode system consisted of a CH Instruments Ag/AgCl reference electrode, platinum counter electrode, and the LIG as the working electrode. CV and EIS experiments were carried out in 10 mL of solution containing 0.1 M KCl, 4 mM K₃[Fe(CN)₆], and 4 mM K₄[Fe(CN)₆]. The scan rates used for CV measurements were 50; 75; 100; 125; 150; 175; and 200 mV s⁻¹, in a sweep range from -0.4 to 0.6 V with a quiet time of 2 s between sweeps. The average sheet resistance, n=3, was taken at ambient conditions (25 °C) on a variable temperature Hall

effect measurement system (model H5000, MMR Technologies, San Jose, CA, USA). EIS analyses were performed in the frequency range of 1 MHz to 100 Hz, using an ac amplitude of 10 mV and a dc voltage of 0 V.

Bacteria Sample Preparation. S. enterica subsp. enterica serovar Typhimurium (ATCC 14028), Bacillus cereus (ATCC 14579), Escherichia coli O157:H7 (ATCC 43895), Listeria monocytogenes (ATCC 15313), Pseudomonas aeruginosa (ATCC 10145), and Staphylococcus aureus (ATCC 29213) were used to test the immunosensor. Bacteria strains stored at -80 °C were resuscitated through two consecutives 24 h growth cycles in TSB at 35 °C. L. monocytogenes were resuscitated under the same time and temperature conditions

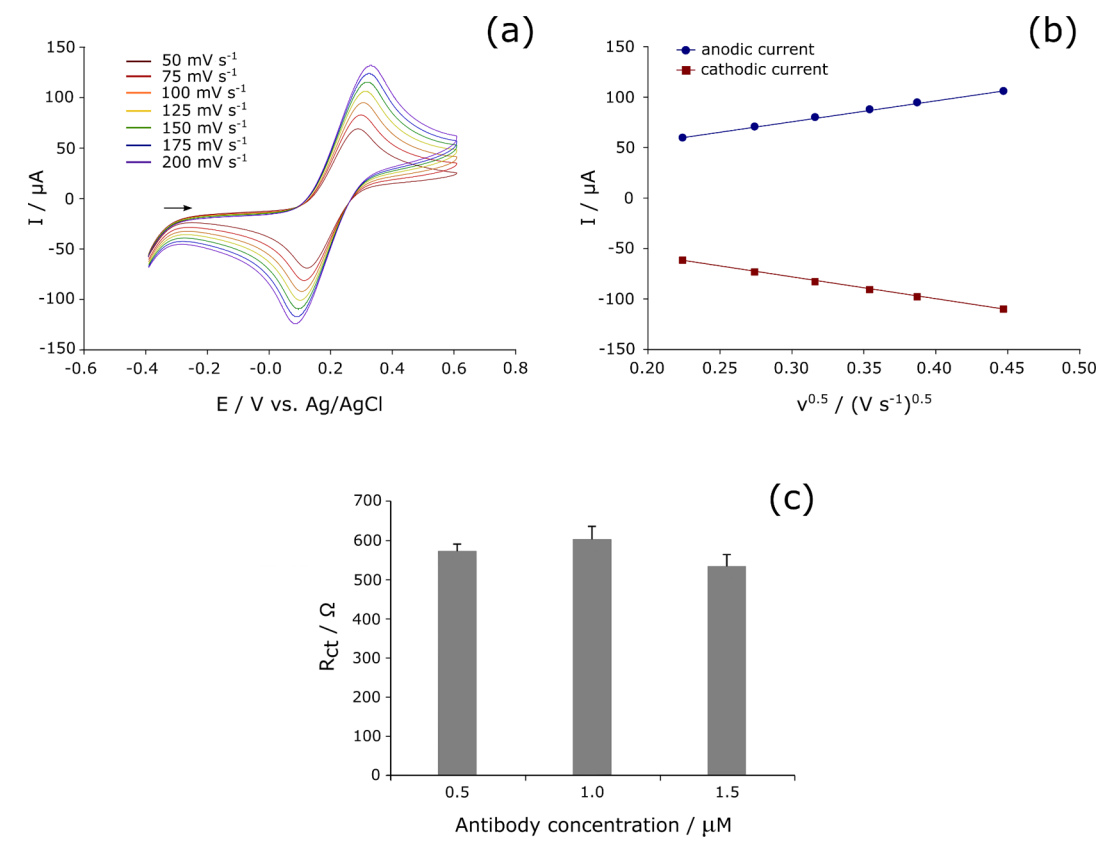


Figure 3. (a) Representative cyclic voltammogram of the LIG electrode vs Ag/AgCl in 0.1 M KCl containing 4 mM $K_3[Fe(CN)_6]/K_4[Fe(CN)_6]$ at scan rates from 50 to 200 mV s⁻¹; (b) Cottrell plot of the LIG electrode vs Ag/AgCl in the same solution at scan rates 50, 75, 100, 125, 150, and 200 mV s⁻¹ with corresponding values of ESA = 0.104 \pm 0.032 cm² and k_0 = 0.0146 \pm 0.0031 cm s⁻¹; and (c) optimization of antibody concentration showing no significant (p > 0.05) difference to R_{ct} variation, according to the Tukey-HSD test. Plot (b) was generated from graph (a) using the method described in the Supporting Information.

in TPB. *B. cereus* was also resuscitated twice in TSB for 24 h but at 30 °C. Bacteria cultures were renewed weekly in TSB or TPB (i.e., one transfer followed by 24 h incubation in aerobic conditions) and maintained at 4 °C. Samples of bacteria were serially diluted in BPW, plated via spread plating on TSA, and incubated for 18 h at 35 or 30 °C before counting the colony growth, and results were reported as CFU mL⁻¹. Different bacteria concentrations, ranging from approximately 25 to 10⁷ CFU mL⁻¹, were prepared in 15 mL of BPW or chicken broth in order to evaluate the impedimetric immunosensor and to simulate its application in food. Plate counting was used parallelly to the immunosensing experiments to confirm the concentration of the bacterial dilutions and validate the impedimetric results.

Bacteria Sensing and Selectivity Test. The presence of bacteria was evaluated by EIS analysis, measuring different bacteria concentrations directly in suspension with an incubation time of 20 min under 180 rpm stirring and an analysis time of 90 s. Before testing the immunosensor in complex media, its performance was verified in pristine buffer, BPW. Between each measurement, the electrode was thoroughly washed with 1× PBS to remove unbound bacteria. Complex plane diagrams (Nyquist plots) were used to determine the charge transfer resistance ($R_{\rm ct}$), the solution resistance ($R_{\rm s}$), the double-layer capacitance ($C_{\rm dl}$), and the Warburg element ($I_{\rm ct}$), fitting the EIS data sets to an equivalent circuit model (i.e., Randles-Ershler circuit) through an EIS spectrum analyzer from ABC Chemistry (Minsk,

Belarus). It should be noted that the diameter of the semicircle obtained from Nyquist plots is a measure of the charge transfer resistance ($R_{\rm ct}$) used to calibrate the concentration of Salmonella attached to the developed biosensor as explained in greater detail in the Results and Discussion section. The LIG-based immunosensor was also evaluated through a selectivity test using the following five food-borne pathogens: E. coli, P. aeruginosa, B. cereus, S. aureus, and L. monocytogenes. These bacteria were chosen because of their importance to food safety and were tested under the same conditions used for S. enterica at a constant concentration of 10^4 CFU mL $^{-1}$.

Data Analysis. The measurements were made in triplicate, and results were expressed as mean \pm standard deviation. Differences between variables were tested for significance using one-way analysis of variance (ANOVA), and significantly, different means (p < 0.05) were designated using Tukey's honestly significant differences (HSD) test through JMP v.13 Software (SAS Institute, Cary, NC, USA). The functional correspondence among quantitative variables was performed using SigmaPlot 12 (Systat, San Jose, CA, USA) by regression analysis. To evaluate the electroactive surface area (ESA) and the heterogeneous electron transfer rate (HET), the peak current values and peak potential separation from the CV results were used to solve the Randles-Sevcik equation 59,66 and to apply the Nicholson method for reversible electron transfers, 70 respectively. The 3σ method was used to calculate the limit of detection (LOD) and sensivity. 59,71 Please see the

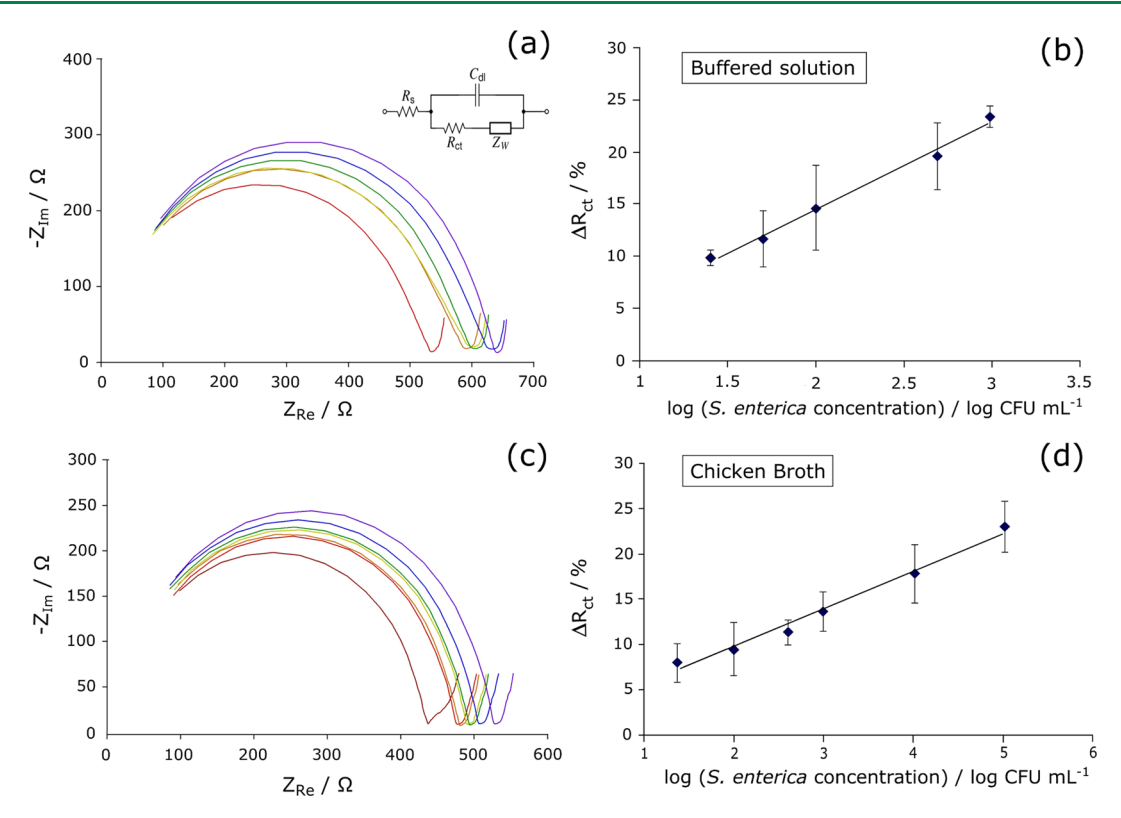


Figure 4. Representative Nyquist plots of impedance spectra of the immunosensor for increasing concentration of *S. enterica* at: (a) 0 CFU mL⁻¹ (red), 29 CFU mL⁻¹ (orange), 63 CFU mL⁻¹ (yellow), 96 CFU mL⁻¹ (green), 512 CFU mL⁻¹ (blue), and 957 CFU mL⁻¹ (purple) in BPW; the inset shows equivalent Randles-Ershler circuit used to fit the curves and to calculate the R_{ct} ; (b) 0 CFU mL⁻¹ (brown), 33 CFU mL⁻¹ (red), 92 CFU mL⁻¹ (orange), 444 CFU mL⁻¹ (yellow), 923 CFU mL⁻¹ (green), 104 CFU mL⁻¹ (blue), and 105 CFU mL⁻¹ (purple) in chicken broth; bacteria concentrations were confirmed by plate counting; the inset shows the equivalent Randles-Ershler circuit used to fit the curves and to calculate the R_{ct} . The linear calibration curve of charge transfer resistance change (ΔR_{ct}) vs *S. enterica* concentrations (log CFU mL⁻¹) in (c) BPW showing a linear regression corresponding to ΔR_{ct} (%) = 8 (concentration of bacteria) + 0.007 with R^2 = 0.984; and (d) in chicken broth with a linear regression corresponding to ΔR_{ct} (%) = 4 (concentration of bacteria) + 0.023 with R^2 = 0.989; data shown as mean ± SD, n = 3. Plots (c,d) were generated from graphs (a,b); respectively.

Supporting Information for further details on calculations and data presentation and analysis.

RESULTS AND DISCUSSION

LIG Electrode Characterization. First, SEM was used to characterize the surface topography of the LIG electrodes (Figure 2a-c). A carbon structure in hexagonal planar configuration was formed, as well as a highly porous 3D electrode rich in edge-plane pyrolytic graphite (EPPG). The cross-sectional image (Figure 2c) shows the LIG electrode as a macroporous/mesoporous structure with a thickness of 15-20 μ m. The irradiation from this laser produced porous graphene onto PI film by converting the carbon from PI into graphitic carbon.⁴⁹ More specifically, the lasing process converts the sp³ carbon into sp² by photothermal effects because of the high temperatures reached at the surface (>1000 °C). As demonstrated in Figure 2a-c, this ablation procedure is able to provide a carbon frame organized into long-range ordered graphene layers.⁷² According to Nayak et al.,⁶⁶ the available edge-plane sites formed on the surface of the LIG electrodes contribute to the electron transfer. The 3D morphology confers a higher and more accessible electrochemical surface area, allowing electrolyte penetration more easily into the active area.

Next, EDS, Raman spectroscopy, and X-ray diffraction (XRD) were performed to analyze the structure of the

materials, as well as the surface molecular groups on the LIG electrode. The C–O, C–N, and C=O bonds originally present in the PI film could easily be broken by the high temperature, ⁴⁹ as confirmed by EDS (Figure 2d). Assuming $(C_{22}O_5N_2H_{10})_n$ as the polymer chain present in the Kapton tape, ⁷³ the initial composition could be calculated to be 69.1, 21.0, 7.3, and 2.6% m/m for C, O, N, and H, respectively, which was converted to 97.5% C and 2.5% O after the lasing process (Figure 2d), with N, H, and O being released as gases because of the high localized heating. ⁴³

Raman spectroscopy was used to determine the graphitic properties of LIG. This technique is also useful to characterize disorder in the resultant sp² carbon lattice. The Raman spectrum showed three main peaks, which is displayed in Figure 2f. The first-order D peak (roughly at 1350 cm $^{-1}$) indicates lattice defects caused by bends or breaks in the sigma bonds; the first-order G peak (roughly at 1580 cm $^{-1}$) shows the lattice vibrations of the sp² carbon atoms while the second-order 2D peak (roughly at 2660 cm $^{-1}$) shows a distinctive peak of graphene structure. The ratio $I_{\rm 2D}/I_{\rm G}$ refers to the number of graphene layers, and according to the obtained ratio $I_{\rm 2D}/I_{\rm G}\approx 0.35$, a multilayer graphene was formed. A expected, these peaks were not observed on the original PI film (Figure 2f). A complementary analysis of LIG electrodes by XRD displayed a peak located at $2\theta=26.5^{\circ}$ (Figure 2e). A very similar result was reported by Nayak et al. Li et al., Li et

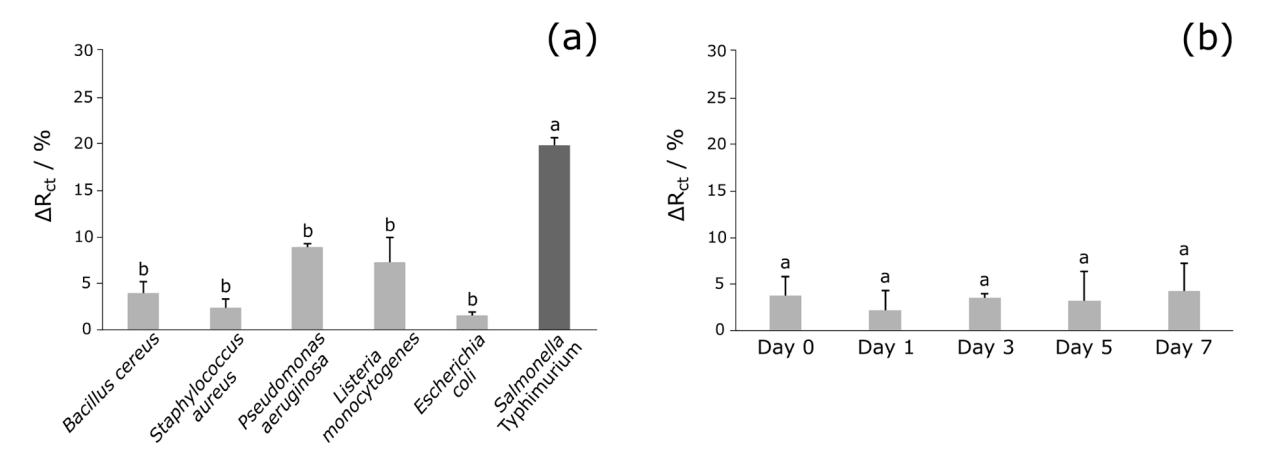


Figure 5. (a) Percentage charge transfer resistance change ($\Delta R_{\rm ct}$ %) versus a constant concentration (10^4 CFU mL⁻¹) of different interferent bacteria and *S. enterica* Typhimurium to show specificity of the immunosensor. A significant change (p < 0.05) in $\Delta R_{\rm ct}$ (%) was observed when *S. enterica* Typhimurium was evaluated (n = 3). Bacteria concentrations were confirmed by plate counting. (b) Stability of the immunosensors during shelf life test for 7 days. Mean values presenting the same lowercase letter are nonsignificantly different, considering a level of significance of 5%. Error bars represent the standard error calculated from three repetitions.

al.,⁴⁹ and Zhang et al.,⁷² indicating the presence of C(002) peak, with an interlayer spacing (I_c) of ~3.36 Å between LIG planes, which indicates a high degree of graphitization.⁴⁹

Electrochemical Characterization. The electrochemical performance of the bare LIG electrodes was investigated in order to verify its ability to act as an electrochemical transducer. CV curves were recorded, and for all scan rates tested, the electrodes displayed well-defined redox peaks (Figure 3a,b), disclosing its quasi-reversible behavior. The change in peak separation ($\Delta E_{\rm p}$ = 166–245 mV) observed from these curves indicated a slower electron transfer rate compared to a reversible system ($\Delta E_p = 60$ mV), which is derived from the presence of defects on the EPPG,66 previously shown by the Raman spectrum (Figure 2f). The electroactive surface area (ESA, 0.104 ± 0.032 cm²) was approximately 50% higher than the geometric area (0.071 cm²), similar to Nayak et al.⁶⁶ findings, who reported ESA = 0.092 ± 0.015 cm² for the same geometric area. This is likely because of the porous graphene structure that increases the surface area, which exposes more edge planes of graphene to the redox solution, helping the electron transfer and, therefore, increases the ESA. 69,7

The CV curves also convey information about the heterogeneous electron transfer rate (HET) between the electrode and the redox mediator species. 66 The HET constant obtained ($k^0 = 0.0146 \pm 0.0031$ cm s⁻¹) exceeds those found by other groups^{59,69,78} ranging from 0.0030 to 0.0044 cm s⁻¹ for LIG with the same redox ferro/ferricyanide species. It also exceeds commercial edge-plane pyrolytic graphite (0.0026 cm s⁻¹) and basal-plane pyrolytic graphite (0.0003 cm s⁻¹), as reported in a previous study by Griffiths et al. These results confirm the effective electron transfer kinetics of LIG produced in this study and its subsequent feasibility for use as an electrochemical transducer. Furthermore, the average sheet resistance of the LIG electrodes was 12.7 \pm 1.6 k Ω sq⁻¹, which is significantly lower than previously reported values of LIGbased electrodes (15–20 $k\Omega$ $sq^{-1})^{60}$ and also lower than electrodes based on inkjet-printed graphene with a reported sheet resistance of 34 k Ω sq⁻¹.⁵² Thus, the results obtained from CV, EIS, and sheet resistance confirm that the LIG electrode fabricated in this study is suitable for electrochemical sensing.

Immunosensor Performance. The bare LIG electrode was converted into an immunosensor by functionalizing the surface with polyclonal antibodies to detect S. enterica Typhimurium via carbodiimide cross-linking (see Material and Methods), as shown in Figure 1. After the functionalization, the R_{ct} values of these electrodes were calculated in order to assess whether changing the antibody concentration would influence its immobilization on the electrode surface. Results showed no significant difference (p > 0.05) among antibody loading concentrations (0.5, 1.0, and 1.5 μ M), with ΔR_{ct} ranging around 1–2% (Figure 3c). Therefore, 1.0 μ M was chosen because it has already been shown in previous studies to obtain a good sensing range.⁷⁹ S. enterica detection was evaluated with EIS, and the change in R_{ct} was used to produce the calibration curve in both BPW and chicken broth. Change in the R_{ct} is proportional to the adhesion of bacterial cells to the biofunctionalized region of the electrode.²² This "biobarrier" hinders the electrolyte access, acting as an electron blocker, therefore increasing the $R_{\rm ct}$ According to this technique, a larger diameter corresponds to a larger R_{ct} , which represents a greater number of bacteria binding to the antibodies on the surface of the electrode. 22 Figure 4 displays the Nyquist plot, a typical impedance spectrum, which shows the increase in R_{ct} with increasing S. enterica concentration, obtained from testing the immunosensor in both suspensions, BPW and chicken broth (Figure 4a,c, respectively). A linear increase in the % $\Delta R_{\rm ct}$ as a function of bacteria concentration is also shown for BPW and chicken broth (Figure 4b,c, respectively).

The presence of attached bacteria cells plays the role of electron kinetic barrier as well as steric hindrance, 20 decreasing the electron transfer path between the electrolyte solution and the electrode, and consequently resulting in the increase of $R_{\rm ct}$ values. A calibration plot was obtained by normalizing the $R_{\rm ct}$ with respect to the $R_{\rm ct}$ value measured for zero concentration of S. enterica in the buffer solution. The LIG-based immunosensor presented a linear sensing range from 25 to 10^3 CFU mL $^{-1}$ ($R^2=0.984$), with a sensitivity of 42 Ω log CFU $^{-1}$ mL and a LOD of 10 CFU mL $^{-1}$ in buffer (Figure 4a,b). To demonstrate the potential of the LIG-based immunosensor in the evaluation of real food samples, chicken broth was used as the sensing matrix. Similarly, a calibration

Table 1. Comparison Among Different Electrochemical Biosensors for Salmonella spp. Detection^a

transducer	material	detection technique	LOD (CFU mL ⁻¹)	working range (CFU mL ⁻¹)	analysis time	sample	refs
GCE	rGO	DPV	10^{1}	$10^1 \text{ to } 10^8$	1 h	chicken in BPW	37
ISE	AuNPs	P	6	$10^1 \text{ to } 10^6$	1 h	PBS, apple juice	67
SPE	rGO	EIS	10^1			water and juice samples	20
SP-IDME	gold	EIS	10^{3}	$10^3 \text{ to } 10^6$	<2 h	chicken rinse water	23
SPE	gold	EIS		$10^3 \text{ to } 10^7$	90 min	redox solution	34
SPE	gold	EIS	10^{3}	$10^3 \text{ to } 10^8$	20 min	PBS, milk	89
SPE	gold	CA	21	$10^1 \text{ to } 10^7$		chicken in liquid samples	31
DWE	CNTs	CA	9	$10^2 \text{ to } 10^7$	6 h	PBS	82
SPE	AuNPs/rGO	DPV	89	$10^2 \text{ to } 10^6$		chicken liver	85
GCE	rGO/MWCNTs	EIS	25	75 to 10 ⁵	1h	chicken	84
IME	Gold/MSNTs	I	500	$10^3 \text{ to } 10^7$	30 min	PBS	90
SPE	gold	CA	10	$10^1 \text{ to } 10^5$	125 min	milk	83
CE	CNWs	i-V	10	$10^1 \text{ to } 10^3$	5 min	beef in BPW	86
GCE	rGO-CNTs	DPV	10	10 ¹ to 10 ⁸	10 min	chicken in BPW	87
LIG	multilayer graphene	EIS	10	$10^1 \text{ to } 10^3$	22 min	BPW	this work
LIG	multilayer graphene	EIS	13	$10^1 \text{ to } 10^5$	22 min	chicken broth	this work

"Glassy carbon electrodes (GCEs), carbon electrodes (CEs), ion selective electrodes (ISEs), screen-printed electrodes (SPEs), screen-printed interdigitated microelectrode (SP-IDME), double-walled electrode (DWE), interdigitated microelectrode (IME), reduced graphene oxide (rGO), gold nanoparticles (AuNPs), carbon nanotubes (CNTs), multiwalled carbon nanotubes (MWCNTs), magnetic silica nanotubes (MSNTs), carbon nanowire (CNW)-buffered peptone water (BPW), phosphate buffered saline (PBS), differential pulse voltammetry (DPV), potentiometry (P), chronoamperometry (CA), impedance (I), and current-voltage (I-V).

plot was obtained by normalizing $R_{\rm ct}$ values with plain chicken broth. Based on the calibration plot, the linear sensing range for *S. enterica* detection in chicken broth was between 25 and 10^5 ($R^2 = 0.989$) with a sensitivity of $24~\Omega$ log CFU⁻¹ mL and a LOD of 13 CFU mL⁻¹ (Figure 4c,d). The total response time for all immunosensing tests was 21.5 min, which consisted of 20 min to allow bacteria contact with the LIG electrode (incubation) and 90 s to collect EIS measurements.

Further, the LIG-based immunosensor was tested for selectivity using five different bacteria strains under the same conditions as those used for *S. enterica* in chicken broth at 10^4 CFU $\rm mL^{-1}$. The $R_{\rm ct}$ values recorded from interference testing did not show significant change among the bacteria tested and presented an average value of 4.8% for the $\Delta R_{\rm ct}$ (Figure 5a). Meanwhile, the average $\Delta R_{\rm ct}$ value for *S. enterica* was 4x higher (19.8%, p < 0.05), emphasizing the specificity of the developed immunosensor to the targeted pathogen (*S. enterica* Typhimurium) and avoiding any false positive signal because of other strains of bacteria that could possibly be non-pathogenic in nature.

The shelf life of freeze-dried immunosensors was evaluated during 7 days of storage at -20 °C (see Supporting Information for details). As it can be observed in Figure 5a, no difference (p > 0.05) was observed in the relative $R_{\rm ct}$ (%) values of the freeze-dried immunosensors. The averaged change in $R_{\rm ct}$ was 3.36%, which demonstrated the stability of the developed immunosensors for at least 7 days. Similarly, absolute $R_{\rm ct}$ (Ω) values before and after the freeze-drying process for each day of analysis did not change significantly (see Figure S1 in Supporting Information). The freeze-drying technique allows the storage of the immunosensor for extended periods of time, which is advantageous for point-of-service applications and crucial for commercialization.

The developed immunosensor exhibited overall good performance using easily obtainable and inexpensive materials with an estimated material cost of \$1.76 per immunosensor (approximate cost breakdown: PI = \$0.15, EDC-NHS = \$0.01, Superblock = \$0.03, ethanolamine = \$0.04, antibodies =

\$1.53), which contributes to its accessible fabrication. Table 1 summarizes the performance characteristics of the immunosensor prepared in this work, as well as other similar biosensors in the recent literature. Previous studies have developed highly sensitive and label-free Salmonella spp. sensors, for example, sensors reported by Silva et al.⁶⁷ and Punbusayakul et al.⁸² based on ion selective electrodes made of gold nanoparticles and double-walled carbon nanotubes, respectively, but all require an hour to multiple hours to obtain a signal, which is longer than 22 min, and the response time is reported herein. Moreover, biosensors that displayed performance similar to this work used expensive materials and/or complex fabrication methods, such as gold^{67,83} or required multistep fabrication to develop the electrodes.⁸⁴ Furthermore, the sensitivity reached by the immunosensor developed herein was significantly higher than other recent graphene-based sensors, even in complex matrices, with a LOD 2× lower than the one obtained by Jia et al.84 and 7× lower than the one obtained by Fei et al. 85 Thiha et al. 86 and Appaturi et al. 87 report impressive analysis times (10 and 5 min, respectively). However, both report the necessity of various pieces of laboratory equipment and chemicals, leading to a much more complex and longer fabrication process than reported in this work. Because this work reports a process that requires only a CO2 laser and a PI substrate for electrode fabrication, it has the advantage of easier upscaling for mass production. These devices also use sample volumes of 5 μ L and 1 mL, which might require sample preconcentration steps to avoid false negatives and consequently increase test response time. Based on the performance characteristics shown in Table 1, there are no concomitant records of a rapid (22 min or less), label-free, sensitive, and simple technique to fabricate sensors similar to the one demonstrated in this work that can selectively detect *S*. enterica from 25 to 10⁵ CFU mL⁻¹, which covers relevant levels for food safety analysis.

CONCLUSIONS

This work reports on a highly sensitive, selective, and easily fabricated impedimetric immunosensor by direct formation of graphene on the commercial PI film through a laser induction technique. The results obtained reinforce that this sensor can be widely implemented because of its simple fabrication protocols with equipment that is accessible throughout the world. This immunosensor is a versatile device that could be distinctly functionalized for monitoring other pathogens besides S. enterica Typhimurium, depending on the selectivity of the biorecognition agent. The working electrode based on LIG displayed a high ESA and HET with values of 0.104 cm² and 0.0146 cm s⁻¹, respectively, and was functionalized with antibodies for S. enterica detection. The immunosensor presented a LOD to the target bacteria of 13 \pm 7 CFU mL⁻¹ in complex media, chicken broth, in just 22 min without any pretreatment. In addition, the sensor exhibited a wide linear sensing range, from 25 to 10⁵ CFU mL⁻¹. Therefore, impedimetric immunosensors based on LIG are very promising for bacteria sensing because it is easily manufactured in ambient conditions compared to other complex fabrication procedures that require CVD⁷⁶ and/or sophisticated substratetransfer techniques, ink and ink-preparation, 52 or postprinting processes.⁵³ Consequently, resulting in a low-cost fabrication process that produces porous graphene with high electrical conductivity and chemical stability.⁸⁸ All of these properties demonstrate that the developed biosensor is well-suited for use in food safety monitoring and, in general, a platform that could be modified with different biorecognition agents for future electrochemical biosensors.

ASSOCIATED CONTENT

Supporting Information

The Supporting Information is available free of charge at https://pubs.acs.org/doi/10.1021/acssensors.9b02345.

Electrochemical surface area calculation; heterogeneous electron transfer rate calculation; determination of LOD; immunosensor shelf life; and immunosensor shelf life results (PDF)

AUTHOR INFORMATION

Corresponding Authors

Jonathan C. Claussen — Department of Mechanical Engineering, Iowa State University, Ames 50011, Iowa, United States; ⊚ orcid.org/0000-0001-7065-1077; Phone: +1 515 294 4690; Email: jcclauss@iastate.edu

Carmen L. Gomes — Department of Mechanical Engineering, Iowa State University, Ames 50011, Iowa, United States; oorcid.org/0000-0003-0095-6478; Phone: +1 515 294 1138; Email: carmen@iastate.edu

Authors

Raquel R. A. Soares — Department of Mechanical Engineering, Iowa State University, Ames 50011, Iowa, United States; Department of Food Technology, Federal University of Viçosa, Viçosa 36570-900, Brazil

Robert G. Hjort – Department of Mechanical Engineering, Iowa State University, Ames 50011, Iowa, United States

Cicero C. Pola – Department of Mechanical Engineering, Iowa State University, Ames 50011, Iowa, United States

Kshama Parate — Department of Mechanical Engineering, Iowa State University, Ames 50011, Iowa, United States Efraim L. Reis — Department of Chemistry, Federal University of Vicosa, Viçosa 36570-900, Brazil

Nilda F. F. Soares — Department of Food Technology, Federal University of Viçosa, Viçosa 36570-900, Brazil

Eric S. McLamore — Agricultural & Biological Engineering, University of Florida, Gainesville 32611, Florida, United States

Complete contact information is available at: https://pubs.acs.org/10.1021/acssensors.9b02345

Notes

The authors declare no competing financial interest.

ACKNOWLEDGMENTS

We gratefully acknowledge funding support from the National Science Foundation under award numbers CBET-1706817, 1512659, 1706994, 1756999, 1805512, and 1511953, and ECCS-1841649. The authors also acknowledge the National Institute of Food and Agriculture, U.S. Department of Agriculture, award numbers 2019-05855 and 2018-672 67016-27578 awarded as a Center of Excellence for financial support. Raquel R.R.A.S. would like to acknowledge the Brazilian National Council for Scientific and Technological Development (CNPq) fellowship (grant #830236/1999-6). We would also like to thank Dr. Loreen Stromberg and Thamires Silva for their help with the experiments.

REFERENCES

- (1) WHO. Executive Summary of Food Borne Diseases -2015. Executive Summary of Food Borne Diseases, 2015; pp 1–2.
- (2) UN/DESA. World Population Prospects 2017—Data Booklet (ST/ESA/SER.A/401); United Nations, Department of Economic and Social Affairs, 2017; pp 1–24.
- (3) FDA. The Reportable Food Registry: A Five Year Overview of Targeting Inspection Resources and Identifying Patterns of Adulteration; U.S. Food and Drug Administration, 2016.
- (4) Centers for Disease Control and Prevention (CDC). An Atlas of Salmonella in the United States, 1968–2011, Atlanta, 2013.
- (5) Maculloch, B.; Hoffmann, S.; Batz, M. B. Economic Burden of Major Foodborne Illnesses Acquired in the United States; CreateSpace Independent Publishing Platform, 2015; Vol. 140, p 59.
- (6) Law, J. W.-F.; Mutalib, N. A.; Chan, K.; Lee, L. Rapid Methods for the Detection of Foodborne Bacterial Pathogens: Principles, Applications, Advantages and Limitations. *Front. Microbiol.* **2015**, *5*, 1–19.
- (7) Clais, S.; Boulet, G.; Van kerckhoven, M.; Lanckacker, E.; Delputte, P.; Maes, L.; Cos, P. Comparison of Viable Plate Count, Turbidity Measurement and Real-Time PCR for Quantification of *Porphyromonas gingivalis*. Lett. Appl. Microbiol. **2015**, *60*, 79–84.
- (8) Wengle, S. When Experimentalist Governance Meets Science-Based Regulations; the Case of Food Safety Regulations. *Regul. Govern.* **2016**, *10*, 262–283.
- (9) Cho, I.-H.; Ku, S. Current Technical Approaches for the Early Detection of Foodborne Pathogens: Challenges and Opportunities. *Int. J. Mol. Sci.* **2017**, *18*, 2078.
- (10) Vanegas, D.; Claussen, J.; McLamore, E.; Gomes, C. Microbial Pathogen Detection Strategies. *Encyclopedia of Agricultural, Food, and Biological Engineering*, 2nd ed.; CRC Press, 2010; pp 1–4.
- (11) Bobrinetskiy, I. I.; Knezevic, N. Z. Graphene-Based Biosensors for on-Site Detection of Contaminants in Food. *Anal. Methods* **2018**, *10*, 5061–5070.
- (12) Sidhu, R.; Rong, Y.; Vanegas, D. C.; Claussen, J.; McLamore, E. S.; Gomes, C. Impedance Biosensor for the Rapid Detection of *Listeria* spp. Based on Aptamer Functionalized Pt-Interdigitated Microelectrodes Array. *Smart Biomedical and Physiological Sensor Technology XIII*, 2016; Vol. 9863, p 98630F.

I

- (13) Hondred, J. A.; Breger, J. C.; Alves, N. J.; Trammell, S. A.; Walper, S. A.; Medintz, I. L.; Claussen, J. C. Printed Graphene Electrochemical Biosensors Fabricated by Inkjet Maskless Lithography for Rapid and Sensitive Detection of Organophosphates. ACS Appl. Mater. Interfaces 2018, 10, 11125–11134.
- (14) Hondred, J. A.; Medintz, I. L.; Claussen, J. C. Enhanced Electrochemical Biosensor and Supercapacitor with 3D Porous Architectured Graphene via Salt Impregnated Inkjet Maskless Lithography. *Nanoscale Horiz.* **2019**, *4*, 735–746.
- (15) Hills, K. D.; Oliveira, D. A.; Cavallaro, N. D.; Gomes, C. L.; McLamore, E. S. Actuation of Chitosan-Aptamer Nanobrush Borders for Pathogen Sensing. *Analyst* **2018**, *143*, 1650–1661.
- (16) Rong, Y.; Padron, A. V.; Hagerty, K. J.; Nelson, N.; Chi, S.; Keyhani, N. O.; Katz, J.; Datta, S. P. A.; Gomes, C.; McLamore, E. S. Post Hoc Support Vector Machine Learning for Impedimetric Biosensors Based on Weak Protein-Ligand Interactions. *Analyst* 2018, 143, 2066–2075.
- (17) Vanegas, D. C.; Gomes, C. L.; Cavallaro, N. D.; Giraldo-Escobar, D.; McLamore, E. S. Emerging Biorecognition and Transduction Schemes for Rapid Detection of Pathogenic Bacteria in Food. *Compr. Rev. Food Sci. Food Saf.* **2017**, *16*, 1188–1205.
- (18) Arora, P.; Sindhu, A.; Dilbaghi, N.; Chaudhury, A. Biosensors as Innovative Tools for the Detection of Food Borne Pathogens. *Biosens. Bioelectron.* **2011**, 28, 1–12.
- (19) Lazcka, O.; Campo, F. J. D.; Muñoz, F. X. Pathogen Detection: A Perspective of Traditional Methods and Biosensors. *Biosens. Bioelectron.* **2007**, 22, 1205–1217.
- (20) Mutreja, R.; Jariyal, M.; Pathania, P.; Sharma, A.; Sahoo, D. K.; Suri, C. R. Novel Surface Antigen Based Impedimetric Immunosensor for Detection of Salmonella typhimurium in Water and Juice Samples. *Biosens. Bioelectron.* **2016**, *85*, 707–713.
- (21) Sheikhzadeh, E.; Chamsaz, M.; Turner, A. P. F.; Jager, E. W. H.; Beni, V. Label-Free Impedimetric Biosensor for *Salmonella* Typhimurium Detection Based on Poly [Pyrrole-Co-3-Carboxyl-Pyrrole] Copolymer Supported Aptamer. *Biosens. Bioelectron.* **2016**, *80*, 194–200.
- (22) dos Santos, M. B.; Azevedo, S.; Agusil, J. P.; Prieto-Simón, B.; Sporer, C.; Torrents, E.; Juárez, A.; Teixeira, V.; Samitier, J. Label-Free ITO-Based Immunosensor for the Detection of Very Low Concentrations of Pathogenic Bacteria. *Bioelectrochemistry* **2015**, *101*, 146–152.
- (23) Xu, M.; Wang, R.; Li, Y. Rapid Detection of Escherichia coli O157:H7 and *Salmonella* Typhimurium in Foods Using an Electrochemical Immunosensor Based on Screen-Printed Interdigitated Microelectrode and Immunomagnetic Separation. *Talanta* **2016**, 148, 200–208.
- (24) Silva, N. F. D.; Magalhães, J. M. C. S.; Freire, C.; Delerue-Matos, C. Electrochemical Biosensors for *Salmonella*: State of the Art and Challenges in Food Safety Assessment. *Biosens. Bioelectron.* **2018**, 99, 667–682.
- (25) Cinti, S.; Volpe, G.; Piermarini, S.; Delibato, E.; Palleschi, G. Electrochemical Biosensors for Rapid Detection of Foodborne *Salmonella*: A Critical Overview. *Sensors* **2017**, *17*, 1910.
- (26) Wang, J. Electrochemical Glucose Biosensors. Chem. Rev. 2008, 108, 814–825.
- (27) Abellán-Llobregat, A.; Jeerapan, I.; Bandodkar, A.; Vidal, L.; Canals, A.; Wang, J.; Morallón, E. A Stretchable and Screen-Printed Electrochemical Sensor for Glucose Determination in Human Perspiration. *Biosens. Bioelectron.* **2017**, *91*, 885–891.
- (28) Lawal, A. T. Progress in Utilisation of Graphene for Electrochemical Biosensors. *Biosens. Bioelectron.* **2018**, *106*, 149–178. (29) Pumera, M. Graphene in Biosensing. *Mater. Today* **2011**, *14*, 308–315.
- (30) Rotariu, L.; Lagarde, F.; Jaffrezic-Renault, N.; Bala, C. Electrochemical Biosensors for Fast Detection of Food Contaminants Trends and Perspective. *Trac. Trends Anal. Chem.* **2016**, *79*, 80–87.
- (31) Salam, F.; Tothill, I. E. Detection of Salmonella typhimurium Using an Electrochemical Immunosensor. *Biosens. Bioelectron.* **2009**, 24, 2630–2636.

- (32) Niyomdecha, S.; Limbut, W.; Numnuam, A.; Kanatharana, P.; Charlermroj, R.; Karoonuthaisiri, N.; Thavarungkul, P. Phage-Based Capacitive Biosensor for *Salmonella* Detection. *Talanta* **2018**, *188*, 658–664.
- (33) Liu, J.; Jasim, I.; Shen, Z.; Zhao, L.; Dweik, M.; Zhang, S.; Almasri, M. A Microfluidic Based Biosensor for Rapid Detection of *Salmonella* in Food Products. *PLoS One* **2019**, *14*, No. e0216873.
- (34) Pagliarini, V.; Neagu, D.; Scognamiglio, V.; Pascale, S.; Scordo, G.; Volpe, G.; Delibato, E.; Pucci, E.; Notargiacomo, A.; Pea, M.; et al. Treated Gold Screen-Printed Electrode as Disposable Platform for Label-Free Immunosensing of Salmonella Typhimurium. *Electrocatalysis* **2019**, *10*, 288–294.
- (35) Cardoso, A. R.; Marques, A. C.; Santos, L.; Carvalho, A. F.; Costa, F. M.; Martins, R.; Sales, M. G. F.; Fortunato, E. Molecularly-Imprinted Chloramphenicol Sensor with Laser-Induced Graphene Electrodes. *Biosens. Bioelectron.* **2019**, *124–125*, 167–175.
- (36) Ye, Y.; Yan, W.; Liu, Y.; He, S.; Cao, X.; Xu, X.; Zheng, H.; Gunasekaran, S. Electrochemical Detection of Salmonella Using an InvA Genosensor on Polypyrrole-Reduced Graphene Oxide Modified Glassy Carbon Electrode and AuNPs-Horseradish Peroxidase-Streptavidin as Nanotag. *Anal. Chim. Acta* 2019, 1074, 80–88.
- (37) Muniandy, S.; Teh, S. J.; Appaturi, J. N.; Thong, K. L.; Lai, C. W.; Ibrahim, F.; Leo, B. F. A Reduced Graphene Oxide-Titanium Dioxide Nanocomposite Based Electrochemical Aptasensor for Rapid and Sensitive Detection of Salmonella enterica. *Bioelectrochemistry* **2019**, *127*, 136–144.
- (38) Lee, J. A.; Hwang, S.; Kwak, J.; Park, S. I.; Lee, S. S.; Lee, K.-C. An Electrochemical Impedance Biosensor with Aptamer-Modified Pyrolyzed Carbon Electrode for Label-Free Protein Detection. *Sens. Actuators, B* **2008**, *129*, 372–379.
- (39) Ping, J.; Zhou, Y.; Wu, Y.; Papper, V.; Boujday, S.; Marks, R. S.; Steele, T. W. J. Recent Advances in Aptasensors Based on Graphene and Graphene-like Nanomaterials. *Biosens. Bioelectron.* **2015**, *64*, 373–385.
- (40) Novoselov, K. S.; Geim, A. K.; Morozov, S. V.; Jiang, D.; Zhang, Y.; Dubonos, S. V.; Grigorieva, I. V.; Firsov, A. A. Electric Field Effect in Atomically Thin Carbon Films. *Science* **2004**, *306*, 666–669
- (41) Balandin, A. A. Thermal Properties of Graphene and Nanostructured Carbon Materials. *Nat. Mater.* **2011**, *10*, 569–581.
- (42) Craciun, M. F.; Russo, S.; Yamamoto, M.; Tarucha, S. Tuneable Electronic Properties in Graphene. *Nano Today* **2011**, *6*, 42–60.
- (43) Kurra, N.; Jiang, Q.; Nayak, P.; Alshareef, H. N. Laser-Derived Graphene: A Three-Dimensional Printed Graphene Electrode and Its Emerging Applications. *Nano Today* **2019**, *24*, 81–102.
- (44) Lee, J.-H.; Park, S.-j.; Choi, J.-W. Electrical Property of Graphene and Its Application to Electrochemical Biosensing. *Nanomaterials* **2019**, *9*, 297.
- (45) Abramova, V.; Slesarev, A. S.; Tour, J. M. Meniscus-Mask Lithography for Narrow Graphene Nanoribbons. *ACS Nano* **2013**, *7*, 6894–6898.
- (46) Abbas, A. N.; Liu, G.; Liu, B.; Zhang, L.; Liu, H.; Ohlberg, D.; Wu, W.; Zhou, C. Patterning, Characterization, and Chemical Sensing Applications of Graphene Nanoribbon Arrays down to 5 nm Using Helium Ion Beam Lithography. *ACS Nano* 2014, *8*, 1538–1546.
- (47) Wei, D.; Liu, Y.; Wang, Y.; Zhang, H.; Huang, L.; Yu, G. Synthesis of N-Doped Graphene by Chemical Vapor Deposition and Its Electrical Properties. *Nano Lett.* **2009**, *9*, 1752–1758.
- (48) El-Kady, M. F.; Strong, V.; Dubin, S.; Kaner, R. B. Laser Scribing of High-Performance and Flexible Graphene-Based Electrochemical Capacitors. *Science* **2012**, 335, 1326–1330.
- (49) Lin, J.; Peng, Z.; Liu, Y.; Ruiz-Zepeda, F.; Ye, R.; Samuel, E. L. G.; Yacaman, M. J.; Yakobson, B. I.; Tour, J. M. Laser-Induced Porous Graphene Films from Commercial Polymers. *Nat. Commun.* **2014**, *5*, 5714.
- (50) Ye, J.; Tan, H.; Wu, S.; Ni, K.; Pan, F.; Liu, J.; Tao, Z.; Qu, Y.; Ji, H.; Simon, P.; et al. Direct Laser Writing of Graphene Made from Chemical Vapor Deposition for Flexible, Integratable Micro-Super-

- capacitors with Ultrahigh Power Output. Adv. Mater. 2018, 30, 1801384.
- (51) Khan, N.; Maddaus, A. G.; Song, E. A Low-Cost Inkjet-Printed Aptamer-Based Electrochemical Biosensor for the Selective Detection of Lysozyme. *Biosensors* **2018**, *8*, 7.
- (52) Torrisi, F.; Hasan, T.; Wu, W.; Sun, Z.; Lombardo, A.; Kulmala, T. S.; Hsieh, G.-W.; Jung, S.; Bonaccorso, F.; Paul, P. J.; et al. Inkjet-Printed Graphene Electronics. *ACS Nano* **2012**, *6*, 2992–3006.
- (53) Das, S. R.; Nian, Q.; Cargill, A. A.; Hondred, J. A.; Ding, S.; Saei, M.; Cheng, G. J.; Claussen, J. C. 3D Nanostructured Inkjet Printed Graphene: Via UV-Pulsed Laser Irradiation Enables Paper-Based Electronics and Electrochemical Devices. *Nanoscale* **2016**, *8*, 15870–15879.
- (54) Parate, K.; Rangnekar, S. V.; Jing, D.; Mendivelso-Perez, D. L.; Ding, S.; Secor, E. B.; Smith, E. A.; Hostetter, J. M.; Hersam, M. C.; Claussen, J. C. Aerosol-Jet-Printed Graphene Immunosensor for Label-Free Cytokine Monitoring in Serum. *ACS Appl. Mater. Interfaces* **2020**, *12*, 8592–8603.
- (55) Secor, E. B.; Prabhumirashi, P. L.; Puntambekar, K.; Geier, M. L.; Hersam, M. C. Inkjet Printing of High Conductivity, Flexible Graphene Patterns. *J. Phys. Chem. Lett.* **2013**, *4*, 1347–1351.
- (56) Secor, E. B.; Gao, T. Z.; Dos Santos, M. H.; Wallace, S. G.; Putz, K. W.; Hersam, M. C. Combustion-Assisted Photonic Annealing of Printable Graphene Inks via Exothermic Binders. *ACS Appl. Mater. Interfaces* **2017**, *9*, 29418–29423.
- (57) Ye, R.; James, D. K.; Tour, J. M. Laser-Induced Graphene. *Acc. Chem. Res.* **2018**, *51*, 1609–1620.
- (58) Chen, Y.; Long, J.; Zhou, S.; Shi, D.; Huang, Y.; Chen, X.; Gao, J.; Zhao, N.; Wong, C. UV Laser-induced Polyimide to Graphene Conversion: Modeling, Fabrication, and Application. *Small Methods* **2019**, *3*, 1900208.
- (59) Vanegas, D.; Patiño, L.; Mendez, C.; Oliveira, D.; Torres, A.; Gomes, C.; McLamore, E. Laser Scribed Graphene Biosensor for Detection of Biogenic Amines in Food Samples Using Locally Sourced Materials. *Biosensors* 2018, 8, 42.
- (60) Garland, N. T.; McLamore, E. S.; Cavallaro, N. D.; Mendivelso-Perez, D.; Smith, E. A.; Jing, D.; Claussen, J. C. Flexible Laser-Induced Graphene for Nitrogen Sensing in Soil. ACS Appl. Mater. Interfaces 2018, 10, 39124–39133.
- (61) Rahimi, R.; Ochoa, M.; Yu, W.; Ziaie, B. Highly Stretchable and Sensitive Unidirectional Strain Sensor via Laser Carbonization. *ACS Appl. Mater. Interfaces* **2015**, *7*, 4463–4470.
- (62) Singh, S. P.; Li, Y.; Be'er, A.; Oren, Y.; Tour, J. M.; Arnusch, C. J. Laser-Induced Graphene Layers and Electrodes Prevents Microbial Fouling and Exerts Antimicrobial Action. *ACS Appl. Mater. Interfaces* **2017**, *9*, 18238–18247.
- (63) Li, L.; Zhang, J.; Peng, Z.; Li, Y.; Gao, C.; Ji, Y.; Ye, R.; Kim, N. D.; Zhong, Q.; Yang, Y.; et al. High-Performance Pseudocapacitive Microsupercapacitors from Laser-Induced Graphene. *Adv. Mater.* **2016**, 28, 838–845.
- (64) Zhang, C.; Xie, Y.; Deng, H.; Tumlin, T.; Zhang, C.; Su, J. W.; Yu, P.; Lin, J. Monolithic and Flexible ZnS/SnO 2 Ultraviolet Photodetectors with Lateral Graphene Electrodes. *Small* **2017**, *13*, 1604197.
- (65) Tao, L. Q.; Tian, H.; Liu, Y.; Ju, Z. Y.; Pang, Y.; Chen, Y. Q.; Wang, D. Y.; Tian, X. G.; Yan, J. C.; Deng, N. Q.; et al. An Intelligent Artificial Throat with Sound-Sensing Ability Based on Laser Induced Graphene. *Nat. Commun.* **2017**, *8*, 14579.
- (66) Nayak, P.; Kurra, N.; Xia, C.; Alshareef, H. N. Highly Efficient Laser Scribed Graphene Electrodes for On-Chip Electrochemical Sensing Applications. *Adv. Electron. Mater.* **2016**, *2*, 1600185.
- (67) Silva, N. F. D.; Magalhães, J. M. C. S.; Barroso, M. F.; Oliva-Teles, T.; Freire, C.; Delerue-Matos, C. *In Situ* Formation of Gold Nanoparticles in Polymer Inclusion Membrane: Application as Platform in a Label-Free Potentiometric Immunosensor for Salmonella typhimurium Detection. *Talanta* **2019**, *194*, 134–142.
- (68) Tehrani, F.; Bavarian, B. Facile and Scalable Disposable Sensor Based on Laser Engraved Graphene for Electrochemical Detection of Glucose. *Sci. Rep.* **2016**, *6*, 27975.

- (69) Fenzl, C.; Nayak, P.; Hirsch, T.; Wolfbeis, O. S.; Alshareef, H. N.; Baeumner, A. J. Laser-Scribed Graphene Electrodes for Aptamer-Based Biosensing. ACS Sens. 2017, 2, 616–620.
- (70) Nicholson, R. S. Theory and Application of Cyclic Voltammetry for Measurement of Electrode Reaction Kinetics. *Anal. Chem.* **1965**, *37*, 1351–1355.
- (71) Taguchi, M.; Schwalb, N.; Rong, Y.; Vanegas, D. C.; Garland, N.; Tan, M.; Yamaguchi, H.; Claussen, J. C.; McLamore, E. S. PulSED: Pulsed Sonoelectrodeposition of Fractal Nanoplatinum for Enhancing Amperometric Biosensor Performance. *Analyst* **2016**, *141*, 3367–3378.
- (72) Zhang, W.; Lei, Y.; Jiang, Q.; Ming, F.; Costa, P. M. F. J.; Alshareef, H. N. 3D Laser Scribed Graphene Derived from Carbon Nanospheres: An Ultrahigh-Power Electrode for Supercapacitors. *Small Methods* **2019**, *3*, 1900005.
- (73) McKeen, L. Polyimides. The Effect of Sterilization Methods on Plastics and Elastomers; Elsevier, 2012; pp 187–204.
- (74) Pimenta, M. A.; Dresselhaus, G.; Dresselhaus, M. S.; Cançado, L. G.; Jorio, A.; Saito, R. Studying Disorder in Graphite-Based Systems by Raman Spectroscopy. *Phys. Chem. Chem. Phys.* **2007**, *9*, 1276–1290.
- (75) Wang, Q. H.; Jin, Z.; Kim, K. K.; Hilmer, A. J.; Paulus, G. L. C.; Shih, C.-J.; Ham, M.-H.; Sanchez-Yamagishi, J. D.; Watanabe, K.; Taniguchi, T.; et al. Understanding and Controlling the Substrate Effect on Graphene Electron-Transfer Chemistry via Reactivity Imprint Lithography. *Nat. Chem.* **2012**, *4*, 724–732.
- (76) Nguyen, V. T.; Le, H. D.; Nguyen, V. C.; Ngo, T. T. T.; Le, D. Q.; Nguyen, X. N.; Phan, N. M. Synthesis of Multi-Layer Graphene Films on Copper Tape by Atmospheric Pressure Chemical Vapor Deposition Method. *Adv. Nat. Sci.: Nanosci. Nanotechnol.* **2013**, 4, 035012.
- (77) Griffiths, K.; Dale, C.; Hedley, J.; Kowal, M. D.; Kaner, R. B.; Keegan, N. Laser-Scribed Graphene Presents an Opportunity to Print a New Generation of Disposable Electrochemical Sensors. *Nanoscale* **2014**, *6*, 13613–13622.
- (78) Abdelbasir, S. M.; El-Sheikh, S. M.; Morgan, V. L.; Schmidt, H.; Casso-Hartmann, L. M.; Vanegas, D. C.; Velez-Torres, I.; McLamore, E. S. Graphene-Anchored Cuprous Oxide Nanoparticles from Waste Electric Cables for Electrochemical Sensing. ACS Sustain. Chem. Eng. 2018, 6, 12176–12186.
- (79) Ohk, S. H.; Koo, O. K.; Sen, T.; Yamamoto, C. M.; Bhunia, A. K. Antibody-Aptamer Functionalized Fibre-Optic Biosensor for Specific Detection of *Listeria monocytogenes* from Food. *J. Appl. Microbiol.* **2010**, *109*, 808–817.
- (80) Ding, S.; Mosher, C.; Lee, X. Y.; Das, S. R.; Cargill, A. A.; Tang, X.; Chen, B.; McLamore, E. S.; Gomes, C.; Hostetter, J. M.; et al. Rapid and Label-Free Detection of Interferon Gamma via an Electrochemical Aptasensor Comprising a Ternary Surface Monolayer on a Gold Interdigitated Electrode Array. ACS Sens. 2017, 2, 210–217
- (81) Ruecha, N.; Shin, K.; Chailapakul, O.; Rodthongkum, N. Label-Free Paper-Based Electrochemical Impedance Immunosensor for Human Interferon Gamma Detection. *Sens. Actuators, B* **2019**, 279, 298–304.
- (82) Punbusayakul, N.; Talapatra, S.; Ajayan, P. M.; Surareungchai, W. Label-Free as-Grown Double Wall Carbon Nanotubes Bundles for Salmonella typhimurium Immunoassay. Chem. Cent. J. 2013, 7, 102.
- (83) Alexandre, D. L.; Melo, A. M. A.; Furtado, R. F.; Borges, M. F.; Figueiredo, E. A. T.; Biswas, A.; Cheng, H. N.; Alves, C. R. A Rapid and Specific Biosensor for *Salmonella* Typhimurium Detection in Milk. *Food Bioprocess Technol.* **2018**, *11*, 748–756.
- (84) Jia, F.; Duan, N.; Wu, S.; Dai, R.; Wang, Z.; Li, X. Impedimetric *Salmonella* Aptasensor Using a Glassy Carbon Electrode Modified with an Electrodeposited Composite Consisting of Reduced Graphene Oxide and Carbon Nanotubes. *Microchim. Acta* **2016**, 183, 337–344.
- (85) Fei, J.; Dou, W.; Zhao, G. Amperometric Immunoassay for the Detection of *Salmonella pullorum* Using a Screen Printed Carbon Electrode Modified with Gold Nanoparticle-Coated Reduced

- Graphene Oxide and Immunomagnetic Beads. *Microchim. Acta* 2016, 183, 757–764.
- (86) Thiha, A.; Ibrahim, F.; Muniandy, S.; Dinshaw, I. J.; Teh, S. J.; Thong, K. L.; Leo, B. F.; Madou, M. All-Carbon Suspended Nanowire Sensors as a Rapid Highly-Sensitive Label-Free Chemiresistive Biosensing Platform. *Biosens. Bioelectron.* **2018**, *107*, 145–152.
- (87) Appaturi, J. N.; Pulingam, T.; Thong, K. L.; Muniandy, S.; Ahmad, N.; Leo, B. F. Rapid and Sensitive Detection of *Salmonella* with Reduced Graphene Oxide-Carbon Nanotube Based Electrochemical Aptasensor. *Anal. Biochem.* **2020**, *589*, 113489.
- (88) Wang, F.; Wang, K.; Zheng, B.; Dong, X.; Mei, X.; Lv, J.; Duan, W.; Wang, W. Laser-Induced Graphene: Preparation, Functionalization and Applications. *Mater. Technol.* **2018**, *33*, 340–356.
- (89) Farka, Z.; Juřík, T.; Pastucha, M.; Kovář, D.; Lacina, K.; Skládal, P. Rapid Immunosensing of *Salmonella* Typhimurium Using Electrochemical Impedance Spectroscopy: The Effect of Sample Treatment. *Electroanalysis* **2016**, 28, 1803–1809.
- (90) Nguyen, P.-D.; Tran, T. B.; Nguyen, D. T. X.; Min, J. Magnetic Silica Nanotube-Assisted Impedimetric Immunosensor for the Separation and Label-Free Detection of Salmonella typhimurium. Sens. Actuators, B 2014, 197, 314–320.